# Characterization of Coal and Biomass Conversion Behaviors in Advanced Energy Systems

**Investigators**
Reginald E. Mitchell, Associate Professor, Mechanical Engineering; Paul A. Campbell and Liqiang Ma, Graduate Researchers

## Introduction

The goal of this project is to develop models that predict accurately coal and biomass gasification and combustion behaviors in the type of environments likely to be established in advanced energy systems. This requires acquiring the information needed to understand and characterize the fundamental chemical and physical processes that govern coal and biomass conversion at high temperatures and pressures. The models can be used to determine operating conditions that optimize thermal efficiency and to examine design strategies for integrating combined cycles for the production of synthesis gas, hydrogen and electric power with minimum impact on the environment.

## Background

The coal-fired power plant will continue to be the workhorse of America's electric power sector for the next 50 years. Improvements in burner designs, refractory materials and high-temperature heat exchangers in combination with hybrid schemes that combine coal combustion and coal gasification have the potential for the development of highly efficient, environmentally clean, power-generating technologies. The increased efficiencies yield lower emissions of greenhouse gases, carbon dioxide emissions being the most critical to reduce. Higher efficiencies also mean that less fuel is used to generate the rated power, resulting in improved system economics.

Biomass is a renewable fuel, and is considered to be $CO_2$-neutral with respect to the greenhouse gas balance if the use of fossil fuels in harvesting and transporting the biomass is not considered. By increasing the fraction of renewable energy in the energy supply, the extent that carbon dioxide emissions will adversely impact the environment can be diminished. Co-firing biomass with coal in traditional coal-fired boilers and furnaces or using biomass-derived gas as a reburn fuel in coal-fired systems represent two options for combined renewable and fossil energy utilization.

Configurations that employ both biomass and coal in integrated gasification combined gas and steam power cycles and hybrid technologies that produce synthesis gas for fuel cells as well as produce electric power in combined gas and steam power cycles offer additional options. Coal and biomass contain significant quantities of hydrogen, and several schemes have been advanced for the efficient and economical production of hydrogen from coal and biomass. With $CO_2$ capture and sequestration, partial coal or biomass oxidation is a promising technology for the production of electric power and hydrogen that uses integrated gasification combined-cycle technology with little adverse environmental impact.

The design of efficient coal/biomass co-utilization energy systems with integrated thermal management to minimize waste heat requires an understanding of the processes that control the physical transformations that coal and biomass particles undergo when exposed to hot environments and the chemical reactions responsible for conversion of the

solid material to gaseous species and ash. The design of efficient systems for the production of hydrogen from coal and biomass also requires an understanding of these physical and chemical processes. The goal of this research project is to provide the needed understanding. Our efforts will result in fundamentals-based sub-models for particle mass loss, size, apparent density, and specific surface area evolution during conversion of coal and biomass materials to gas-phase species during gasification and combustion processes.

During this final, close-out period of the project, we have (i) updated our mode of burning model to reflect our recent modifications to the reduced heterogeneous reaction mechanism employed in the model; (ii) used a detailed, comprehensive heterogeneous reaction mechanism to characterize the impact of the migration of surface oxides during the char oxidation process; (iii) used the model to characterize the impact of pressure on the mode of burning; and (iv) collected samples of chars created under high-pressure conditions in our high-pressure reaction chamber that was developed over the course of this project. The chars are to be examined in order to characterize the impact of pressure on char-particle morphology. An overview of the activities associated with these research areas follows.

**Discussion of Significant Results**

*Characterization of Char-Particle Burning Behavior*

Several studies have shown that during the combustion of coal particles in conditions typical of those existing in industrial, pulverized coal-fired boilers and furnaces, char particles burn at rates limited by the combined effects of chemical reaction and pore diffusion. Due to the oxygen concentration gradients established inside particles and the associated distribution of rates of mass loss due to chemical reaction, particle diameters, apparent densities, and specific surface areas decrease with mass loss when burning is in this regime. The char conversion model that we have developed accounts for these variations in the physical structure of the char during the mass loss process.

The equations that constitute the char conversion model were presented in the previous annual report to GCEP. In the direct numerical simulation of a burning spherical char particle, the particle is divided into a number of concentric annular volume elements, each of which contains a portion of the initial total mass of the particle. The mass in each volume element gasifies at a rate governed by the local conditions. An oxygen transport equation is solved to determine the oxygen concentration in each volume element. Account is made for the combined effects of bulk and Knudsen diffusion of oxygen through pores, surface roughness, the local porosity, and the particle tortuosity when evaluating an effective diffusivity for oxygen inside the particle. The local adsorption rate of $O_2$ is dependent on the local adsorbed oxygen concentration and the available surface area within the volume element, which is followed using a specific surface area sub-model. As carbon oxides desorb from the surface as CO and $CO_2$, the local particle density decreases and the local porosity increases. As conversion progresses, eventually all the mass in the volume element is consumed. Since the oxygen concentration is highest at the particle periphery, reactivity is greatest near the particle perimeter and mass in the outer-most volume element can be consumed prior to complete mass loss in inner volume elements. Consequently, the particle diameter can decrease as burning progresses.

Char-particle temperature is calculated from an energy balance, wherein the rates of energy generation due to char oxidation are balanced by the rates of energy loss by conduction, convection, and radiation. Particles are assumed to burn at uniform temperature, an adequate assumption for the small particles sizes (< 150 μm) for which the model is applicable.

During the past year, we modified the reduced heterogeneous reaction mechanism employed in the model in order to better reflect our understanding of the chemistry controlling the carbon oxidation process. The modified mechanism, shown in the Table I, accounts for the early $CO_2$ evolution observed during the oxidation of some coal chars and nearly all biomass chars.

**Table I:** Reduced heterogeneous reaction mechanism

| | | $A_i$ [a] | $\bar{E}_i$ (kJ/mol) | $\sigma_i$ (kJ/mol) |
|---|---|---|---|---|
| $2\,C_f + O_2 \rightarrow C(O) + CO$ | (R1a) | 3.87e04 | 60 | 0 |
| $\rightarrow C_2(O_2)$ | (R1b) | 1.95e03 | 55 | 0 |
| $C_b + C_f + C(O) + O_2 \rightarrow CO_2 + C(O) + C_f$ | (R2) | 1.18e09 | 120 | 0 |
| $C_b + C_f + C(O) + O_2 \rightarrow CO + 2C(O)$ | (R3) | 3.74e16 | 250 | 0 |
| $C_b + C(O) \rightarrow CO + C_f$ | (R4) | 1.00e13 | 320 | 26 |
| $C_b + C_2(O_2) \rightarrow CO_2 + 2C_f$ | (R5) | 1.00e13 | 280 | 45 |

[a] $k_i = A_i \exp\left(-E_i / \hat{R}T\right)$, *units of* $A_i$ *in mol,* $m^2$*-surface/*$m^3$*-fluid, s*

In the mechanism, $C_f$ represents a free carbon site, one available for oxygen adsorption, and C(O) and $C_2(O_2)$ represent adsorbed oxygen atoms, one oxygen atom per carbon site. In accord with the type oxide complexes identified by Zhuang *et al.* [1] on carbon surfaces during oxidation, the complex C(O) is representative of carbonyl- and ether-type complexes (the desorption of which leads to CO), and $C_2(O_2)$ is representative of lactone- and acid anhydride-type complexes (the desorption of which leads to $CO_2$). So that the reactions are balanced, bulk carbon atoms, $C_b$, are shown; they are assumed to have unity activity. Reaction R1 (represented by reactions R1a and R1b) is assumed to have two product channels, one leading to the formation of C(O) and the other, to $C_2(O_2)$. Reactions R1b and R5 were included to account for the significant quantities of $CO_2$ observed in temperature programmed desorption (TPD) tests performed in our laboratory and in the TPD tests of Sokova [2].

Also in our modified approach, the rates of Reactions (4) and (5) were modeled using a distributed activation energy approach in order to account for the variations in the strengths of adsorbed oxygen atoms. Temperature programmed desorption experiments were used to determined mean activation energies and standard deviations for use in a Gaussian distribution. Using the rate parameters shown in the table, CO and $CO_2$ release rates and mass loss rates during TPD experiments and during oxidation tests are accurately characterized for the char employed in the tests.

*Detailed Heterogeneous Oxidation Mechanism*

The heterogeneous oxidation mechanism described above is a reduced mechanism, one having sufficient detail to describe the dominant chemical pathways during the carbon oxidation process but simple enough to use in the type DNS calculations required for the mode of burning model. This reduced mechanism is derived from analysis of a detailed reaction mechanism that accounts for oxygen physisorption and chemisorption, surface oxide migration, and carbon oxide desorption. In the detailed mechanism, a distribution of oxygen complexes are involved in all reactions to reflect the impact of the distribution of the strengths of all oxygen complexes formed on the carbonaceous surface. The detailed mechanism is shown in Table II, below.

**Table II:** Detailed heterogeneous reaction mechanism

$$\text{-C} + \text{O}_2 \underset{phy,b}{\overset{phy,f}{\rightleftharpoons}} \text{-C-}(\text{O}_2) \quad \text{(R1)}$$

$$\text{-C-}(\text{O}_2) + \text{-C} \xrightarrow{chm0} \text{-C}(\text{O}^{\text{m}}) + \text{-C}(\text{O}^{\text{m}}) \quad \text{(R2)}$$

$$\text{-C-}(\text{O}_2) + \text{-C} + \text{-C-} \xrightarrow{chm1} \text{CO} + \text{-C}(\text{O}^{\text{m}}) + \text{-C} \quad \text{(R3)}$$

$$\text{-C-}(\text{O}_2) + \text{-C} + \text{-C-} \xrightarrow{chm2} \text{CO}_2 + \text{-C} + \text{-C} \quad \text{(R4)}$$

$$\text{-C-}(\text{O}_2) + \text{-C}(\text{O}) + \text{-C-} \xrightarrow{chm3a} \text{CO} + \text{-C}(\text{O}^{\text{m}}) + \text{-C}(\text{O}^{\text{m}}) \quad \text{(R5a)}$$

$$\text{-C-}(\text{O}_2) + \text{-C}_2(\text{O}_2) + \text{-C-} \xrightarrow{chm3b} \text{CO} + \text{-C}(\text{O}^{\text{m}}) + \text{-C}(\text{O}^{\text{m}}) + \text{-C}(\text{O}^{\text{m}}) \quad \text{(R5b)}$$

$$\text{-C-}(\text{O}_2) + \text{-C}(\text{O}) + \text{-C-} \xrightarrow{chm4a} \text{CO}_2 + \text{-C}(\text{O}^{\text{m}}) + \text{-C} \quad \text{(R6a)}$$

$$\text{-C-}(\text{O}_2) + \text{-C}_2(\text{O}_2) + \text{-C-} \xrightarrow{chm4b} \text{CO}_2 + \text{-C}(\text{O}^{\text{m}}) + \text{-C}(\text{O}^{\text{m}}) + \text{-C} \quad \text{(R6b)}$$

$$\text{-C}(\text{O}^{\text{m}}) \xrightarrow{mig1} \text{-C}(\text{O}) \quad \text{(R7)}$$

$$\text{-C}(\text{O}^{\text{m}}) + \text{-C}(\text{O}) \xrightarrow{mig2a} \text{-C}_2(\text{O}_2) \quad \text{(R8a)}$$

$$\text{-C}(\text{O}^{\text{m}}) + \text{-C}_2(\text{O}_2) \xrightarrow{mig2b} \text{-C}_2(\text{O}_2) + \text{-C}(\text{O}) \quad \text{(R8b)}$$

$$\text{-C}(\text{O}) \xrightarrow{mig3a} \text{-C}(\text{O}^{\text{m}}) \quad \text{(R9a)}$$

$$\text{-C}_2(\text{O}_2) \xrightarrow{mig3b} \text{-C}(\text{O}^{\text{m}}) + \text{-C}(\text{O}) \quad \text{(R9b)}$$

$$\text{-C}(\text{O}) + \text{-C-} \xrightarrow{\text{des1}} \text{CO} + \text{-C} \quad \text{(R10)}$$

$$\text{-C}_2(\text{O}_2) + \text{-C-} \xrightarrow{\text{des2}} \text{CO}_2 + \text{-C} + \text{-C} \quad \text{(R11)}$$

For every carbon gasified, an underlying bulk carbon -C- is brought to the surface. The complex -C($O^m$) represents migrating chemisorbed oxides. Multiple forward arrows for reaction progress represent reactions that proceed according to the distributive nature of a reactant species.

The char oxidation mechanism comprises fourteen distinct reactions. In some reactions, the reactant is a single-oxygen oxide site, -O, and the kinetics of the reaction is assumed to be independent of oxide's association, whether belonging to -C(O) or $-C_2(O_2)$. These almost-duplicate reactions are suffixed with "a" and "b". When such duplicates are considered, the mechanism reduces to eleven reactions. In terms of the 11-step form of the mechanism, physisorption is defined by one reversible reaction, (R1); chemisorption consists of five reactions, three with free-site reactants, (R2) – (R4), and two with stable-oxide-site reactants, (R5) and (R6); migration has three reactions, (R7) – (R9); and desorption is defined by reactions (R10) and (R11).

The kinetic parameters determined for a synthetic char are shown in Table III. The use of a synthetic char in this phase of the project permitted the study of the char oxidation process without the possible catalytic effects of ash and without the complications of unknown chemical composition and unknown porosity inherent in real coals and biomass. Oxidation tests in a variety of environments differing in temperature and composition in our pressurized thermogravimetric analyzer (PTGA) were used to determine the kinetic parameters. Monitored during the gravimetric tests were mass loss, gas-phase CO and $CO_2$ concentrations, and adsorbed oxygen concentrations. In selected tests, *in situ* specific surface areas were also measured.

**Table III:** Kinetic parameters determined for synthetic char

| Reaction | $A$ ($s^{-1}$, $m^3 \cdot mol^{-1}$, $m^2 \cdot mol^{-1}$) | $b$ | $E_o$ (kJ/mol) | $\omega^a$ (kJ/mol) | $a^a$ |
|---|---|---|---|---|---|
| (R1) | $2.40 \times 10^5$ | 0.5 | 0 | - | - |
| (R-1) | $1.15 \times 10^{14}$ | - | 50 | - | - |
| (R2) | $8.73 \times 10^{12}$ | - | 137 | 60 | 1 |
| (R3) | $1.00 \times 10^{21}$ | - | 310 | 150 | 1 |
| (R4) | $2.61 \times 10^{14}$ | - | 154 | 150 | 10 |
| (R5)[b] | $3.94 \times 10^{17}$ | - | 206 | - | - |
| (R6)[b] | $1.98 \times 10^{17}$ | - | 195 | - | - |
| (R7) | $1.00 \times 10^{17}$ | - | 23 | - | - |
| (R8)[b] | $8.95 \times 10^{11}$ | - | 18 | - | - |
| (R9)[b] | $3.98 \times 10^{05}$ | - | 200 | - | - |
| (R10) | $1.00 \times 10^{13}$ | - | 150, 480 | - | - |
| (R11) | $1.00 \times 10^{13}$ | - | 114, 365 | - | - |

Elovich-type kinetics were assumed for certain reactions to account for free-site population distributions and to empirically reproduce the trends of decreasing chemisorptivity with increasing surface coverage. Traditionally, Elovich-type models assume a linear dependence between surface coverage and activation energy. While allowing for this possibility, this study suggests that as surface coverage increases, the

activation energy of adsorption may approximately asymptote to the mode-average activation energy of the free-sites. As the most chemisorptive sites are occupied, the remaining sites tend to differ less from each other, leading to a more constant activation energy at higher coverages. This effect was only observed for reaction (R4) and not for reactions (R2) and (R3), suggesting that $CO_2$ formation favors the most chemisorptive free-sites, and dominates chemisorption until the inhibitory effects of stable oxides on these sites restrains the process.

An example of comparisons of the results of the PTGA oxy-reactivity experiments with the results of the numerical model, based on the suggested mechanism and parameters, are shown in Fig. 1.

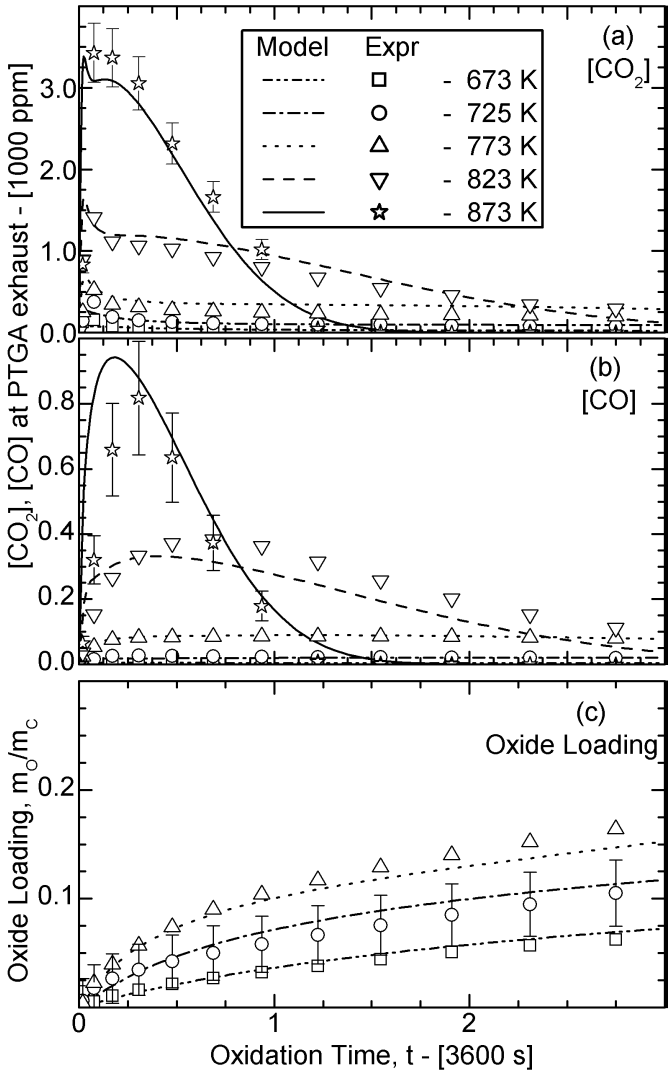


**Figure 1.** Comparison of model results with experimental results of the char oxidation process in the PTGA. Shown are (a) the $CO_2$ concentration in PTGA exhaust gases, (b) the CO concentration in PTGA exhaust gases, and (c) the oxide loading on char sample.

With the detailed heterogeneous reaction mechanism, we were able to assess the role of surface migration on carbon reactivity. Evolution rates of CO and $CO_2$ for a temperature programmed desorption (TPD) experiment are shown in Fig. 2. Model calculations simulating the TPD experiment are also shown. Without migration, simulated gas evolution rates resemble a Gaussian shape. However, a bimodal $CO_2$ evolution profile and slightly right-skewed CO evolution profile were experimentally observed. Similar bimodal profiles were observed by Skokova [2], who demonstrated the significance of migration during char oxidation and its effect of increasing overall $CO_2$ formation. Building on this foundation, the current results demonstrate that migration is not only responsible for increased total $CO_2$ production, but for the bimodal nature of the $CO_2$ evolution profiles as well.

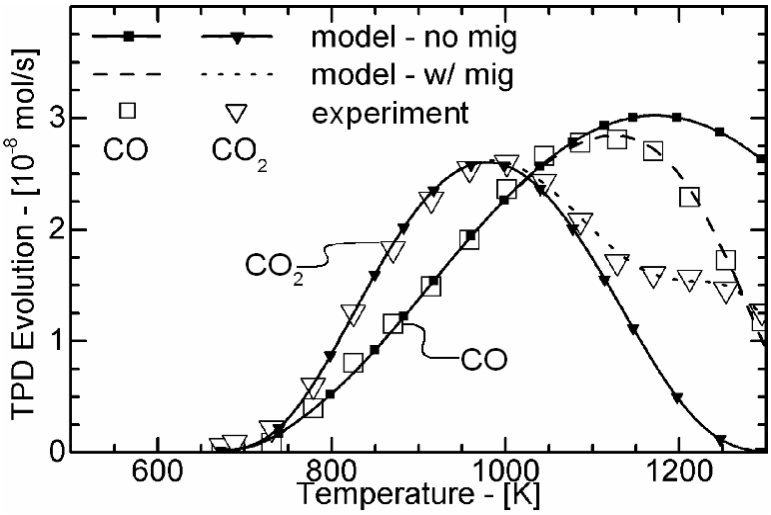


**Figure 2:** Comparison of TPD experimental results versus model results, and the effect of neglecting migration.

The detailed mechanism has provided considerable insight into the chemical pathways that are important in the carbon oxidation process. It has been quite useful in helping to define the reduced mechanism that is used in our char conversion models.

*Impact of Pressure on Char Conversion*

Pressurized gasification and combustion of fossil fuels have the advantages of increased conversion efficiency, decreased pollutant emissions, and reduced reactor furnace size. Characterizing the impact of pressure on char conversion was one of the goals of this project. To this end, we have undertaken experiments to increase the data available on the conversion rates of coal chars at elevated pressures and have used the data, supplemented with calculations, to characterize the separate effects of total pressure and oxygen mole fraction on char reactivity in the type environments likely to be established in advanced energy systems.

Pressure influences both chemical reaction rates and the rate of oxygen transport to the particle's outer surface and through the particle's pores. Consequently, understanding the impact of pressure on char conversion rates requires understanding the impact of pressure on both chemistry and mass transport.

The impact of pressure on char conversion rates depends upon the particle temperature. At relatively low temperatures when chemical reaction rates are slow compared to mass transport rates ($T_p$ < ~900 K), oxygen completely penetrates the particle and the particle burns in the so-called Zone I burning regime in which char conversion rates are controlled by the rates of chemical reactions. In this regime, pressure impacts reaction rates only to the extent that it impacts the partial pressure of oxygen ($P_{O2} = y_{O2}P$). Thus, for fixed oxygen mole fraction, if pressure is increased the partial pressure of oxygen is increased, increasing chemical reaction rates, and the time for complete char conversion decreases. At sufficiently high particle temperatures when reaction rates are fast compared to mass transport rates ($T_p$ > ~ 1800 K), oxygen is consumed at the particle periphery, and the particle burns in the so-called Zone III burning regime in which char conversion rates are controlled by the rate that oxygen diffuses to the outer surface of the particle. Bulk diffusion coefficients are inversely proportional to pressure, thus at high temperatures, for fixed oxygen mole fraction if pressure is increased, oxygen transport rates decrease and the time for complete conversion of the char increases.

In the Zone II burning regime (~900 K < $T_p$ < ~1800 K), the combined effects of chemical reaction and mass transport control char conversion rates. Both Knudsen and bulk diffusion can control the rate that oxygen diffuses through the particle, depending upon the pore size. In small pores, Knudsen diffusion dominates, and oxygen transport is independent of pressure. As conversion progresses and pores merge and coalesce becoming larger, bulk diffusion inside particles becomes ever more rate-controlling, and oxygen transport rates decrease as pressure is increased.

Char reactivities at different total pressures and constant oxygen partial pressure for a synthetic char burning in the Zone I regime were determined from measurements, and are plotted in Fig. 3. For an oxygen partial pressure of 0.24 atm and temperatures of 723 and 773 K, the reaction rates are nearly the same during the whole range of conversion.

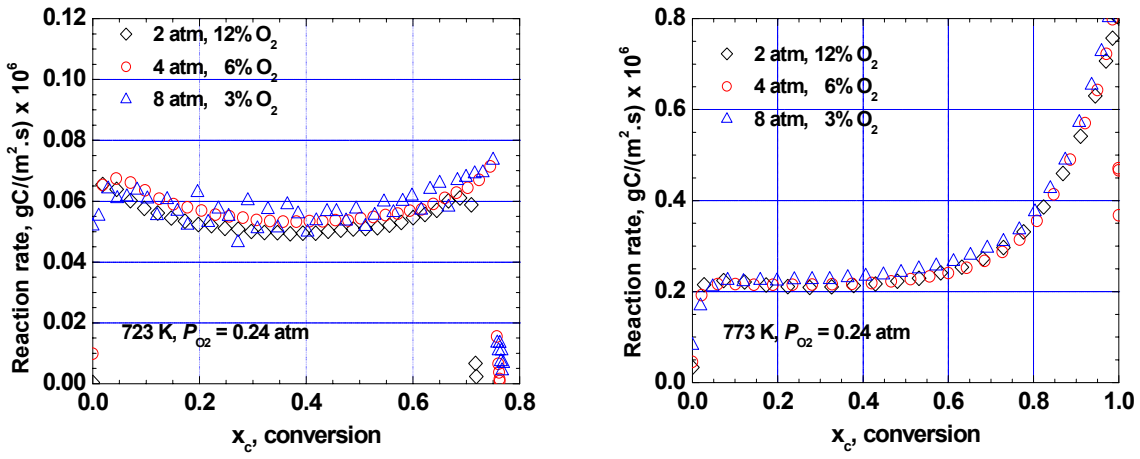


**Figure 3.** Effect of total pressures (2, 4 and 8 atm) on reaction rate at constant oxygen partial pressure ($P_{O2}$ = 0.24 atm) for a 16% porosity synthetic char.

This effect of total pressure on reactivity with constant oxygen partial pressure throughout the conversion of the char was also simulated with the model, and the results are shown in Fig. 4. For an oxygen partial pressure of 0.06 atm, total pressures of 1, 5, 10, and 20 atm, and gas temperature of 873 K, the reactivities are the same during the whole range of conversion. This implies that at a given temperature, char reactivity is determined solely by the oxygen partial pressure ($P_{O2} = y_{O2}P$), independent of the individual values of total pressure $P$ and oxygen mole fraction $y_{O2}$ when burning is chemical kinetically controlled. Calculations indicate that for fixed oxygen mole fraction and gas temperature, particle temperatures remain relatively constant as pressure is increased for Zone I burning.

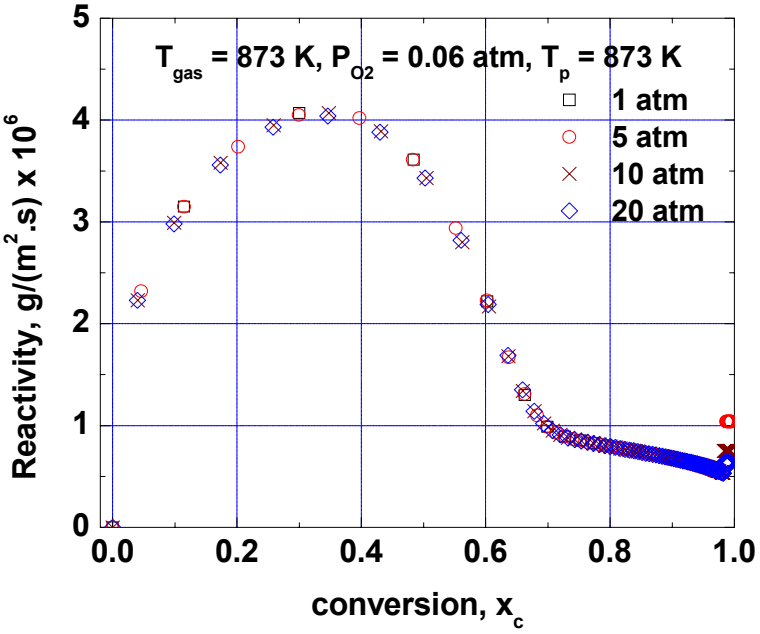


**Figure 4.** Reactivity as a function of conversion with constant oxygen partial pressure at different total pressures (1, 5, 10 and 20 atm) and gas temperature of 873 K.

Of particular interest is the instantaneous apparent reaction order, $n$, a measure of the sensitivity of the char reactivity to the oxygen partial pressure:

$$n \equiv \left[ \frac{\partial \ln\left(\bar{R}_{i,C}\right)}{\partial \ln\left(P_{O_2}\right)} \right]_{T,P}$$

Calculations indicate that under Zone I burning conditions, $n$ is a function of $T$, $P$ and $y_{O2}$, and is not a constant over the whole range of oxygen partial pressures as suggested in many studies. Calculations indicate that the value of $n$ increases with oxygen partial pressure and that $n\left(P_{O_2,2}\right)_{T_p,P} > n\left(P_{O_2,1}\right)_{T_p,P}$ when $P_{O_2,2} > P_{O_2,1}$. When comparing the values of $n$ at a fixed oxygen partial pressure for different temperatures within the Zone I regime,

calculations indicate that the rate of reactivity increase with respect to oxygen partial pressure is lower at higher temperature, *i.e.*, $n(T_2)_{P_{O_2},P} < n(T_1)_{P_{O_2},P}$ if $T_2 > T_1$.

The effect of increasing oxygen partial pressure at a constant gas temperature and total pressure is shown in Fig. 5 for Zone II-type burning. Although the gas temperature was held constant in these calculations ($T_{gas}$ = 1600 K), the particle temperature during the burnout increased in response to the increasing oxygen partial pressure. Therefore, the increase in reactivity is partially due to the increased particle temperature.

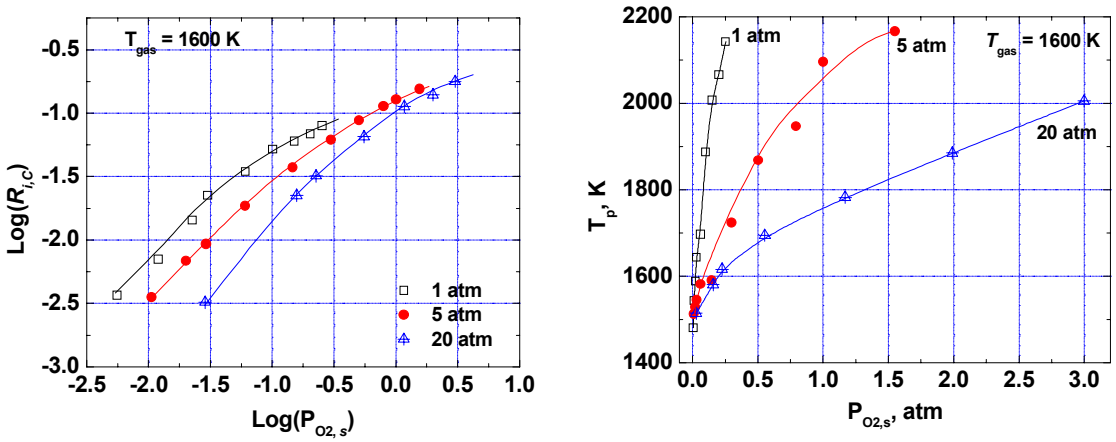


**Figure 5.** Calculated variation of reactivities and particle temperatures with respect to oxygen partial pressure at particle surface at gas temperature of 1600 K.

Values for *n* can be determined from the slopes of the curves in Fig. 5. Under Zone II burning conditions, such as at 1600 K, the value of *n* is not a constant over the whole range of oxygen partial pressure studied, and is pressure dependent. Although there is an almost constant value of *n* for low values of the oxygen partial pressure at the particle surface $P_{O2,s}$, *n* tends to decrease with increase in $P_{O2,s}$. This trend differs from that observed under Zone I burning conditions, in which *n* increases with increasing oxygen partial pressure. It is clear that the decrease in the value of *n* is due to pore diffusion limitations.

The dependence of reactivity and particle temperature on total pressure when oxygen partial pressure remains fixed is presented in Fig. 6. In the Zone I burning regime, such as at 873 K, the reactivity is independent of total pressure as long as the oxygen partial pressure is held constant and the average particle temperature is the same as gas temperature. At low temperature, when burning occurs in Zone I, the reactivity is solely determined by chemistry, and diffusion limitation will not come into play, even at elevated pressures. At high temperatures ($T_{gas}$ = 1600 K), the burning is restricted to the periphery of the particle (strong Zone II). Under strong Zone II burning conditions, both the reactivity and average particle temperature decrease with total pressure. In the strong Zone II burning regime, the reactivity is controlled by both chemistry and pore diffusion during the whole conversion of the material, even at atmospheric pressure. With elevated pressures, the molecular diffusivity decreases, rendering the impact of diffusion limitation on reactivity more significant. When the pore diffusion rate has decreased to a certain extent, external bulk diffusion will become the controlling factor on reactivity,

and burning enters the Zone III burning regime. At moderate gas temperatures ($T_{gas}$ = 1140 K), there is significant internal burning at nearly constant diameter up to certain extents of conversions (weak Zone II). Under weak Zone II burning conditions, the reactivity also decreases with total pressure but at a slower rate. Weak Zone II is a situation in between Zone I and strong Zone II, where the material burns in Zone I at early conversions and in Zone II in later conversions. The overall effect is that as pressure increases, the chemical rate controlling steps become less important, and diffusion control becomes more significant.

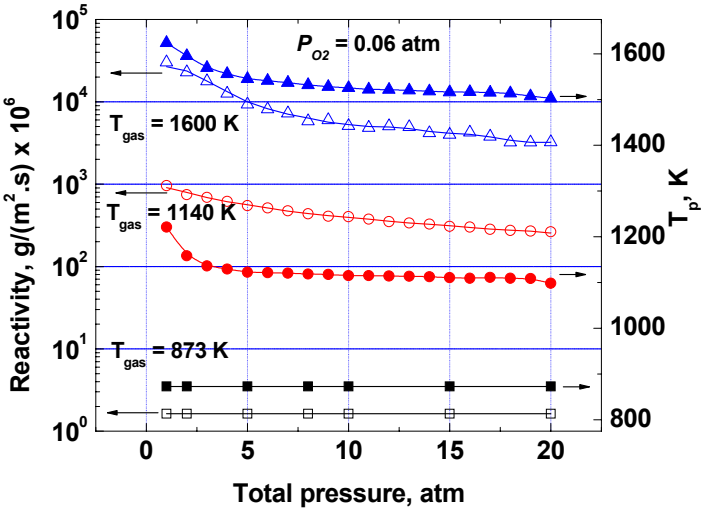


**Figure 6.** The dependence of reactivity and particle temperature on total pressure with constant oxygen partial pressure (0.06 atm) at different gas temperatures (873, 1140 and 1600 K).

Since over a range of total pressure the molecular diffusivity is inversely proportional to total pressure and Knudsen diffusivity is independent of total pressure, pore diffusion limitation becomes more significant at elevated pressures. However, in Zone II burning with fixed oxygen partial pressure, the reactivity is lower at higher total pressure. With fixed temperature and oxygen partial pressure, the burning regime could change from Zone I to Zone II as the total pressure increases.

At constant gas composition, the total effect of increasing total pressure is to increase the reactivity, with a trade-off between higher chemical reaction rates due to a higher oxygen concentration and a proportionately lower diffusion coefficient. This effect is weak (in weak Zone II) or negligible (strong Zone II) at pressures above 10 atm. The critical pressure where the particle temperature levels off is lower at higher gas temperature. At fixed oxygen partial pressure, the transition temperature from Zone I to Zone II is lower at higher total pressure.

*High-Pressure Chars*

Pressure influences coal swelling and the yields of volatiles during devolatilization. Consequently, pressure influences the structure and morphology of the char produced. Pulverized coal char particles produced at high heating rates and high pressures have a morphology that is more cenospheric in character than chars produced at atmospheric

pressure. Low to medium porosity particles having large voids inside their outer walls, both single-cavity and multiple-cavity and thin-walled and thick-walled, are produced at elevated pressures, the higher the pressure, the thinner the walls and the fewer the cavities. Because of these differences in char structure, in the same oxidation environment, a char produced at a high pressure will lose its mass at a faster rate than a char produced at a lower pressure.

During the course of this project, we have designed, fabricated, and constructed a pressurized chamber that encloses the entrained flow reactor that we use in our high-temperature oxidation tests. The pressurized facility allows high-pressure oxidation tests up to 50 atm to be performed, permitting the investigation of the effects of pressure on coal conversion rates under conditions typical of high-pressure/high-temperature industrial furnaces and boilers.

To date, we have collected chars produced by devolatilizing raw feed stocks at elevated pressures. These chars are being examined to determine their morphologies, and are presently being subjected to tests to determine their specific surface areas and reactivities to oxygen. We are also modifying our particle population balance model to include particles differing in morphology, characterized as being either dense particles or thin-walled or thick-walled cenospheres,

**Progress**

Considerable progress has been made towards developing the understanding needed to predict the behaviors of coal and biomass chars during conversion in high-temperature, high-pressure environments. Presently, we are capable of characterizing accurately the chemical and physical changes that coal and biomass char particles undergo during conversion in combustion and gasification conditions likely to occur in advanced energy conversion systems. The models that we have developed constitute sub-models that can be used in more comprehensive models developed to investigate potential design strategies and to help define optimum operating conditions that yield high coal and biomass conversion efficiencies with minimum impact on the environment.

**Future Plans**

Studies to determine the relationship between model parameters and coal and biomass properties are ongoing as are studies to characterize the impact of the ash-content of particles on char reactivity. We will use our high-pressure facility to observe Zone II burning behaviors at elevated pressures and to obtain char samples in our efforts to characterize reactivity differences due to morphological changes that occur as a consequence of devolatilization at high pressures. The studies undertaken will help us understand how coal and biomass properties influence char conversion rates in high-temperature, high-pressure environments.

**Publications**

The following papers were presented at conferences during the past year:

1. Saarenpaa, I., Mitchell, R. E., and Ma, L. “Overlap of Devolatilization and Char Oxidation during Combustion of Pulverized Biomass Particles under Oxygen-Enriched Conditions,” Swedish-Finnish Flame Days 2005, Borås, Sweden, October 18-19, 2005.

2. Ma, L. and Mitchell, R. E., "The Effects of Total Pressure and Oxygen Partial Pressure on Char Reactivity," 2006 Spring Meeting, Western States Section of the Combustion Institute, Boise State University, Boise, Idaho, March 27-28, 2006.

The following papers have been prepared for publication, and will be submitted to journals before the end of May:

1. Campbell, P. A., Mitchell, R. E., and Ma, L. "Impact of Distributed Surface-Oxides and their Migration on the Heterogeneous Carbon-Oxygen Mechanism," to be sent to *Comb & Flame* in May 2006.
2. Mitchell, R. E., Ma, L. and Kim, B. J. "On the Burning Behaviors of Pulverized Coal and Biomass Chars," to be sent to *Energy & Fuels* in May 2006.

**References**

1. Zhuang, Q. L., Kyotani, T. and Tomita, A. *Energy Fuels* **8** 714 (1994).
2. Skokova, K. A., *Selectivity in the Carbon-Oxygen Reaction (Heteroatoms)*, Ph.D. Thesis, The Pennsylvania State University, State College, PA, 1997.

**Contact**

Reginald E. Mitchell: remitche@stanford.edu